Since January 2020 Elsevier has created a COVID-19 resource centre with free information in English and Mandarin on the novel coronavirus COVID-19. The COVID-19 resource centre is hosted on Elsevier Connect, the company's public news and information website.

Biosensors and Bioelectronics 98 (2017) 292–298

Contents lists available at ScienceDirect

Biosensors and Bioelectronics

journal homepage: www.elsevier.com/locate/bios

Electrochemical nucleic acid detection based on parallel structural dsDNA/recombinant azurin hybrid

Mohsen Mohammadniaei[a,1], Taek Lee[a,b,1], Jinho Yoon[a], Donghyun Lee[c,*], Jeong-Woo Choi[a,*]

[a] Department of Chemical and Biomolecular Engineering, Sogang University, 35 Baekbeom-ro (Sinsu-dong), Mapo-gu, Seoul 121-742, Republic of Korea
[b] Department of Chemical Engineering, Kwangwoon University, 20 Kwangwoon-Ro, Nowon-Gu, Seoul 01897, Republic of Korea
[c] School of Integrative Engineering Chung-Ang University, Heukseok-dong, Dongjak-gu, Seoul 156-756, Republic of Korea

ARTICLE INFO

Keywords:
Nucleic acid detection
Electrochemical biosensor
Parallel structural dsDNA
DNA conductance
MiRNA detection
DNA conductance

ABSTRACT

Several challenges remained to fabricate a molecular-level nucleic acid biosensor such as surface immobilization control, single mismatch detection and low current response. To overcome those issues, for the first time, authors presented a novel parallel structural dsDNA/recombinant azurin (PSD/rAzu) hybrid structure for the general nucleic acid detection. The PSD was designed and introduced by the optimized 8 Ag^+ ions to have greater conductivity than the canonical dsDNA, and conjugated with rAzu to develop a general platform for electrochemical detection of miRNAs and viral DNAs with high reproducibility and ultra-sensitivity towards single base pair mutation. Thanks to the bifunctional rAzu as the selective spacer and electrochemical signal mediator, in the presence of the target strand, the imperfect PSD switched rapidly to the upright position where the Ag^+ ions intercalated between C-C mismatches of dsDNAs at the top of each structure brought further from the electrode surface resulting in a significant electrochemical signal drop of the Ag^+ ions. The charge transfer (CT) mechanism across the hybrid structure was simply clarified on the basis of the redox potential location of the species. The electrical conductivity of DNAs were measured using scanning tunneling spectroscopy (STS) at the molecular scale and cyclic voltammetry (CV) technique based on the reduction of Ag^+ ion. The proposed PSD/rAzu hybrid structure with a great capability of single mutation recognition and miRNA expression level profiling in cancer cells holds a very promising platform to be studied for further development of various kinds of nanoscale biosensors, bioelectronic devices.

1. Introduction

Development of a highly reproducible and reliable nucleic acid biosensor platform to screen genetic disorders caused by base pair mutation is crucial for early-stage diagnosis of different types of disease (Baker, 2006; Choi et al., 2016; Drummond et al., 2003). Among them, the other nucleic acids such as microRNAs (miRNAs) as short noncoding RNAs 19–25 nucleotides long) are important because of their functions in regulation of diverse gene expressions and involvement in tumor initiation, metastasis and apoptosis (He et al., 2005; Ma et al., 2016). Unusual expression of distinctive miRNAs associated with various human cancers has made these biomolecules important clinical biomarkers (Calin and Croce, 2006; O'Connell et al., 2008). Commonly used miRNA sensors are known as Northern blotting and real-time PCR which offer great sensitivities (Catuogno et al., 2011; Nolan et al., 2006; Válóczi et al., 2004). Despite their complexity and high cost, however, sophisticated primer design and the necessity process of reverse transcription used in PCR for small RNA targets cause extra errors, nonspecific binding and low primer hybridization efficiency (Wu and Qu, 2015). Alternatively, signal-amplifying mechanisms such as loop-meditated isothermal amplification (LAMP) (Li et al., 2011), catalyzed hairpin assembly (Jiang et al., 2014), rolling circle amplification (Cheng et al., 2009), bio-barcode gel assay (Lee et al., 2014) and strand displacement (Walker et al., 1992) can truly increase the miRNA detection sensitivity and specificity, but require multiple and complex detection processes together with various enzymes or reagents. Thus, new methods were developed to reduce those tedious procedures, for example fluorescence (Yin et al., 2012), surface enhanced Raman spectroscopy (Wang et al., 2016a), electrochemiluminescence (Feng et al., 2016), surface plasmon resonance (Wang et al., 2016b) and electrochemistry (Labib et al., 2016). Among them, electrochemical-based biosensors have received much attentions due to their simplicity, low cost and high sensitivity for the detection of short RNAs and viral DNAs (Campuzano et al., 2014; Wu and Qu, 2015). For instance, aloe-like gold micro/nanostructures (Shi et al., 2013), three-mode system (Labib et al.,

* Corresponding authors.
E-mail addresses: dhlee@cau.ac.kr (D. Lee), jwchoi@sogang.ac.kr (J.-W. Choi).
[1] These authors contributed equally to this work.

http://dx.doi.org/10.1016/j.bios.2017.07.005
Received 16 April 2017; Received in revised form 22 June 2017; Accepted 4 July 2017
Available online 05 July 2017
0956-5663/

2013), hybridization chain reaction (Ge et al., 2014), target recycling (Wu et al., 2015), 3 C strategy (Chen et al., 2016) and protein electrocatalysis (Labib et al., 2015). Although they have made great analysis advances, but still require special nanostructured electrode or need labeling mediators for sensitive detection which such agents hamper target binding and reduce specificity and/or require complicated and multistep detection process (details of previous reports are provided in table S1), also the reproducibility of electrochemical biosensors have remained challenging.

To address those issues, several platforms have been reported to improve the reproducibility and fidelity of electrochemical biosensors. Surface treatment and functionalization preserves an important role to prevent non-specific bindings, physical adsorptions and provide sufficient spacing in solution phase to better the sensing performance and achieve a high-throughput target analysis. Aniline derivative electro-addressing mechanism (Corgier et al., 2007) was reported to solve the aforementioned problems but it is still unable to provide enough spacing for target invasion. The emerging 9 G DNA chip (Song et al., 2011), offering a 2D microarray, roughly addressed those issues but limited to control the orientation of DNA strands. Nanocones (dendrons) surface modification (Hong et al., 2005), Strepdavidin-Biotin immobilization, (Dupont-Filliard et al., 2001) and DNA-nanostructured scaffold (Lin et al., 2016) because of their 3D structure have been proposed to remove all those challenges but the non-conductive function of those microarray molecules affects the sensitivity of biosensors, also the orientation control is not resolved properly.

To overcome reproducibility and multiplicity problems, we employed recombinant azurin (rAzu) immobilized on the gold electrode to provide a stable anchoring site which removed the requirements of additional linkers and functioned as a selective-arrayed molecule because of its appropriate cross-sectional diameter (~5 nm) and ability to receive only one DNA strand at its N-terminus. Also, to eliminate the monotonous multiplex detection procedures and reduce the detection time, in the present study, a novel structure composed of parallel structural dsDNA (PSD) and rAzu was proposed as a general platform for the precise detection of short nucleic acids such as miRNAs and viral DNAs in single step with high specificity towards single base pair mutation in 1 h (Fig. 1). The PSD structure resembling a parallel electrical circuit, was designed and implemented as a DNA wire with greater electrical conductivity than conventional dsDNA and provided a remarkable platform for the detection of single mismatched mutation at very low concentration. A silver ion intercalated between C-C mismatched base pairs at the top of each structure acted as the signal reporter for electrochemical conductance measurement and target detection. The CT ability of rAzu based on the Cu^{+}/Cu^{2+} redox reaction seemed to play a significant role in CT modulation and controlling the charge migration across the structure. Also at pH 7.4, rAzu molecules with an isoelectric point of 6.03 offered a negatively-charged surface, which caused DNA strands (negatively-charged backbone) to be arranged vertically, hence, eliminating the lateral DNA adsorptions to the surface. The developed structure was applied for electrochemical detection of miRNA-155, which is overexpressed in MDA-MB-231 breast cancer cells and underexpressed in A549 lung cancer cells (Jiang et al., 2005; Lee et al., 2014; Roa et al., 2010). Also for the versatility test, it was employed for the detection of various miRNAs and viral DNAs such as miRNA-21, miRNA-141, miRNA-143, MERS-CoV and HIV-1 viruses. Furthermore, the proposed PSD biosensor showed a good capability towards monitoring the miR-155 expression levels in two different cancer cell lines.

2. Result and discussion

2.1. Conformation analysis of PSD/rAzu hybrid

The TBM-native polyacrylamide gel electrophoresis (PAGE), scanning tunneling microscopy (STM), flow surface plasmon resonance (F-SPR) and CV techniques were used to confirm the PSD structures. In the PAGE analysis (Fig. 2a), the bands in lanes I and III corresponded to miR-155 (R) and 22 bp ssDNA (T_1) were different due to self-aggregation of RNA strands, resulting in slow migration. Similar bands were seen from 66 bp ssDNAs (D_1 and D_2) in lanes II and IV. Lanes V and VI indicate that the target miR-155 hybridized to the T_2 strand with high specificity. The smeared band may be due to bending tendency of RNA which forces DNA strand to form different structures leading different migration velocity inside the gel. The imperfect PSD is

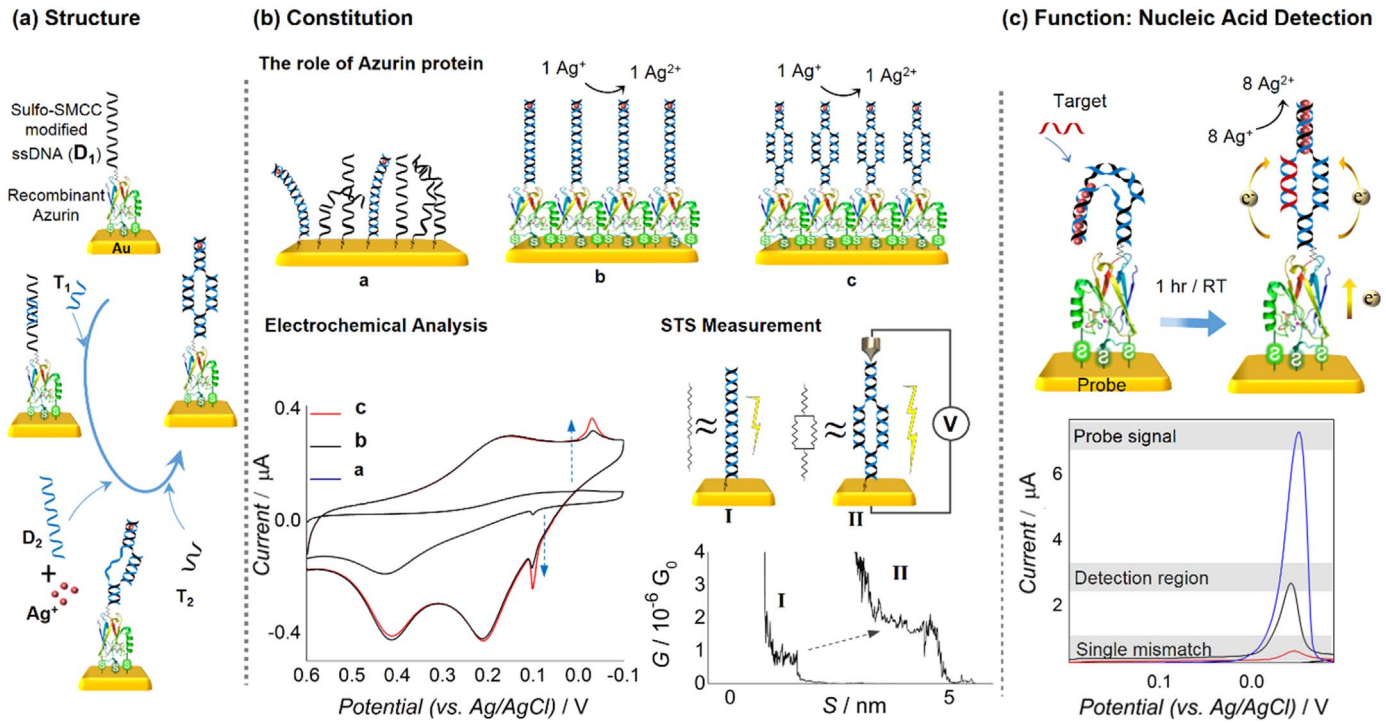

Fig. 1. Schematic diagram of Parallel Structural dsDNA (PSD) adsorbed onto recombinant azurin (PSD/rAzu). (a) Immobilization process of the whole structure, (b) constitution towards the role of rAzu and DNA conductance enhancement, (c) Function of PSD for nucleic acid detection.

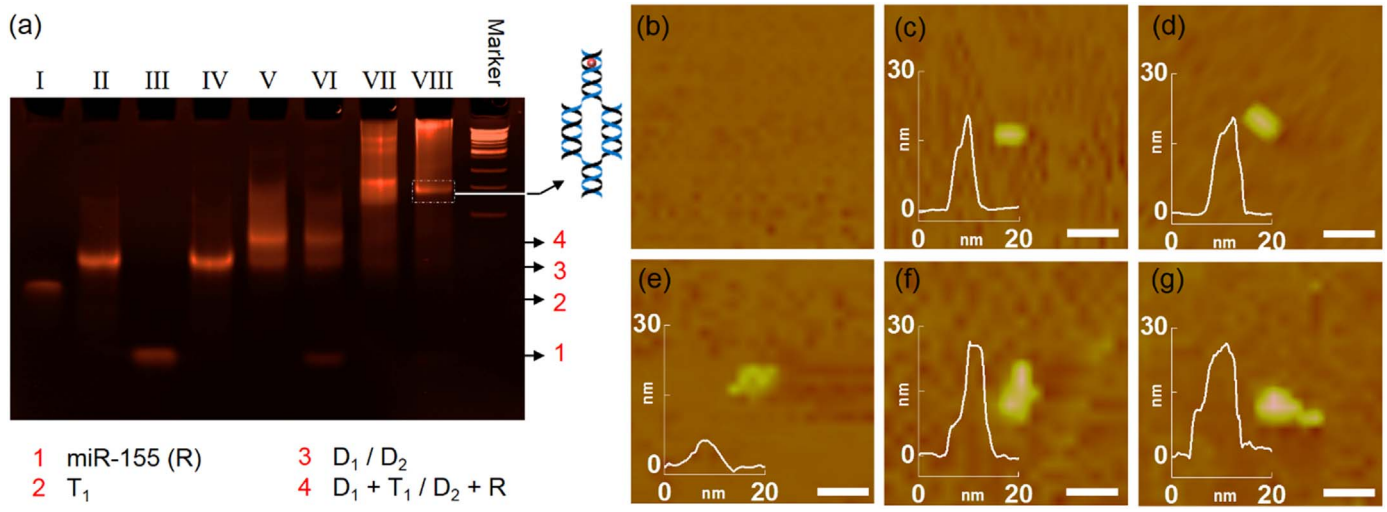

Fig. 2. Structure conformation analysis. (a) Native polyacrylamide gel (12% TBM) with ethidium bromide staining for PSD conformation analysis. (I) R, (II) D_2, (III) T_1, (IV) D_1, (V) D_2+R, (VI) D_2+R+T_1, (VII) D_2+T_1+D_1, and (VIII) D_2+R+T_1+D_1. The last lane is a 100 base pair DNA marker. STM analysis of morphological image and the corresponding cross-sections for: (b) bare Au electrode, (c) dsDNA, (d) PSD, (e) rAzu, (f) dsDNA/rAzu, and (g) PSD/rAzu. Scale bar is 10 nm. The STM images were recorded in air with tunneling current of 1 nA and bias of 100 mV.

shown in lane VI, in which the bands are smeared and not well separated. In lane VII, a well-defined band before the 200 bp marker confirms the PSD structure (176 bp). Smeared bands in both VI and VII lanes might result from the fact that, since the structure is in the solution state, alongside the parallel structure (PSD) there is a possibility of formation of secondary structures and self-aggregation of imperfect PSD also existence of macro molecules such as tetra, hexa and octa structures. As a result, the layer-by-layer self-assembly of the PSD was studied, since the thiolated-ssDNA is priory immobilized and fixed to the substrate not to allow the secondary structures occurrence.

For the layer-by-layer self-assembly study of the hybrid structure at the molecular scale, STM measurement was carried out. Fig. 2b-d illustrated a morphological image of five studied structures of dsDNA, PSD, rAzu, dsDNA/rAzu and PSD/rAzu along with the corresponding cross-section of each individual samples which clarifies the conformation of complex structure.

For further confirmation of the PSD/rAzu structure, flow surface plasmon resonance (F-SPR), CV and electrochemical impedance spectroscopy (EIS) measurements were also performed (see the Supplementary information (S. 4, 5, 6) and Figs. S2, 3, 4).

2.2. The role of recombinant azurin towards DNA electrochemical signal enhancement

Various metalloprotein-based bioelectronic devices have been developed in our group to make these materials very practical candidates in this area (Choi et al., 2007; Chung et al., 2015; Lee et al., 2010; Yagati et al., 2013), from which, we used rAzu containing three cysteine residues, produced by the site-directed mutagenesis technique (Kafi et al., 2016; Lee et al., 2011). The role of rAzu on DNA electrochemical signal was investigated based on the reduction of Ag^+ ions, covalently bound between dsDNA mismatches (C-Ag^+-C), (Ono et al., 2008) which was designed to be located at the top of the each dsDNAs (Fig. 1a). Electrodes were prepared (Supplementary information (S. 7) and Fig. S5) and directed to the electrochemical cell as the working electrodes then potential was scanned negatively (forward scan). Cathodic currents were detected, resulting from the reduction of silver ions upon the application of a sufficiently negative potential, indicating a CT yield across the complex. It is worth saying that, the occurrence of the silver ion reduction potential after that of the copper ion and DNA (Fig. 3a, b) confirms the CT direction from gold substrate to silver ion through the complex. Also, compared to the previously reported methods (Inouye et al., 2005; Slinker et al., 2010; Wohlgamuth et al., 2013) for electrochemical DNA CT analysis using redox dyes such as Nile blue, Redmond Red and Ferrocene with broad redox signals, in our approach silver ions remove the requirement for DNA labeling, and yield a very sharp, distinctive and well-localized cathodic peak, which enables signal detection at a very low target concentration (Fig. 3b). Therefore, silver ion can be a well-defined redox reporter candidate for DNA electrochemical signal analysis.

To better understand the complex CT kinetics, a set of experiments were conducted at a very low DNA concentration (0.5 μM) with high accuracy. Analysis was conducted in the absence (no C-C mismatch) and presence of Ag^+ ions (C-1Ag^+-C mismatch). As seen in Fig. 3a, in the absence of Ag^+ ions, the electrochemical signal of dsDNA adsorbed by rAzu immobilized on Au electrode (dsDNA/rAzu) was higher than the direct adsorbed one. A shift in redox potentials and currents of DNA and rAzu in different configuration states was observed. The reduction potential (E_{pc}) of azurin (182 ± 24 mV) occurred before that of the dsDNA (144 ± 12 mV), but in the conjugation state, the dsDNA-E_{pc} and azurin- E_{pc} were accumulated, leading to a higher i_{pc} while their oxidation potentials were well-distinctive. In addition, a considerable increase in dsDNA-i_{pc} (25 ± 3 nA to 94 ± 6 nA) alongside a shift in oxidation potential (E_{pa}) from 228 ± 24 mV to 401 ± 26 mV and a dramatic increase in dsDNA-i_{pa} (−25 ± 4 nA to 156 ± 8 nA) were evident. Similarly, the role of rAzu in redox signal enhancement of Ag^+ ions (i_{pc}: 11 ± 2 nA to 33 ± 4 nA and i_{pa}: −14 ± 2 nA to −37 ± 5 nA) and dsDNA (i_{pc}: 24 ± 4 nA to 107 ± 3 nA and i_{pa}: −23 ± 4 nA to −89 ± 6 nA) was observed (Fig. 3b).

Although, it seemed the observed electrochemical signal enhancement of DNA was resulted from the well-controlled number of immobilized DNA molecules. Whereas this is in contradiction with the fact that, rAzu was expected to execute an extra resistance to the structure and increases the distance of Ag+ ions from the surface leading to a lower conductivity of dsDNA. The rationale behind this phenomenon might be schematically explained in Fig. 3c. By driving the electrode to more negative potentials, the energy of the electrons is increased. They can reach a level high enough to transfer into vacant electronic states on species in the electrolyte (Path No. 1) (Bard and Faulkner, 2000). Since the reduction potential of rAzu takes place before that of Ag^+ and approximately before dsDNA (Fig. 3a and b), application of a negative potential scan on the working electrode results in electrons traveling from the Au electrode to rAzu, causing the copper

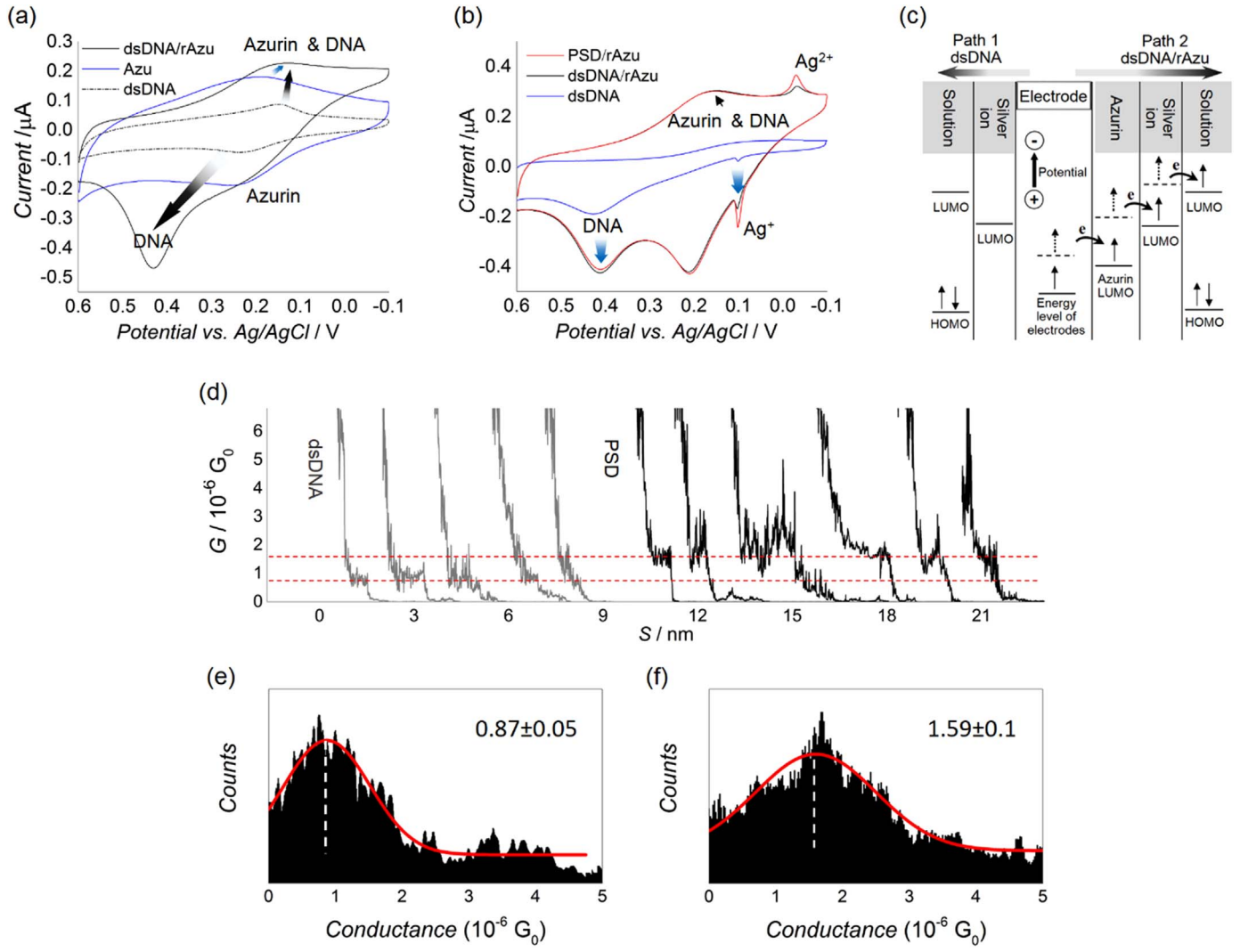

Fig. 3. Electrochemical and electrical analysis. (a) CV obtained from dsDNA (dash line), rAzu (blue line), and dsDNA/rAzu, in the absence of Ag^+. (b) CV response of the C-1Ag^+-C dsDNA (blue line), C-1Ag^+-C dsDNA/rAzu (black line), and C-1Ag^+-C PSD/rAzu, in the presence of Ag^+. Oligonucleotides' concentration: 0.5 p.M., rAzu: 0.100 mg mL^{-1}. CV Data are based on the 10th cycle. (c) Schematic diagram showing the intuition behind CT in the dsDNA and dsDNA/rAzu with C-1Ag^+-C. (d) Examples of the conductance vs. tip separation scans, showing the conductance steps for dsDNA (fist five curves from the left) and PSD (six curves from the right) which are immobilized onto Au electrode. The experiments were performed at current set point of 0.5 nA and bias voltage of −0.3 V. Conductance histograms and the Gaussian distribution curves for (e) dsDNA and (f) PSD. The histograms have taken from 500 experimental curves, extracted from at least 10 similar I-V curves of different samples after bare electrode signal subtraction. The measurements is limited by a 1 GΩ series resistor. The measured DNA molecules were topographically scanned before and after I-V measurement, to confirm whether or not the structures remain intact and that the STM tip position was not changed.

ion to be reduced first. Electrons then transfer across the DNA strand and reduce silver ions, leading a higher cathodic current of Ag^+ compared with the dsDNA/Au electrode structure. In other words, electrons are more likely to travel through path number 2, where the vacant molecular orbits are in a lower energy state. More interestingly, azurin protein caused DNA to have a higher electrochemical signal, which confirms that azurin protein is a pronounced electron donor to DNA and increases its conductance. Thus, rAzu behaves as an electron donor, the DNA helix as a charge mediator and silver ion as an electron acceptor.

2.3. Comparison between dsDNA and PSD using electrochemical analysis

Comparing the conductance of the proposed PSD and dsDNA based on the conventional Au electrodes in an electrochemical cell necessitates very high accuracy. Due to the lateral size differences between PSD and dsDNA (~4 and ~2 nm, respectively), controlling the number of molecules to be identical per area of electrode was necessary to compare their conductance. As seen in schematic diagram of Fig. S6, in order to immobilize PSD on Au electrode using self-assembly method, after ssDNA immobilization, there should be enough space for the other three strands to incorporate into the structure and form the final PSD. Notably, mercaptoethanol as the spacer cannot provide a sufficient space between the ssDNAs resulting an inaccurate control in the number of immobilized molecules onto the surface. Therefore, rAzu was used as a selective molecule to receive DNA molecules (Supporting information, S. 8).

If we simply assume the 66 bp dsDNA as a classical wire with a defined resistance, then, the total dsDNA of 66 bp is defined as three 22 bp helixes with same electrical resistance (R), in a series connection depicted in Fig. 1b. PSD would correspond to a combined circuit comprising series and parallel circuits. According to Ohm's law (Millikan and Bishop, 1917), in the case of PSD, there are four resistances that two of them are in parallel to give a total resistance of 2.5 R while it is 3 R in dsDNA. Supposing that each individual part has the same length and cross-sectional area, the conductivity of PSD should increase by 20%. As shown in Fig. 2a, the reduction current of

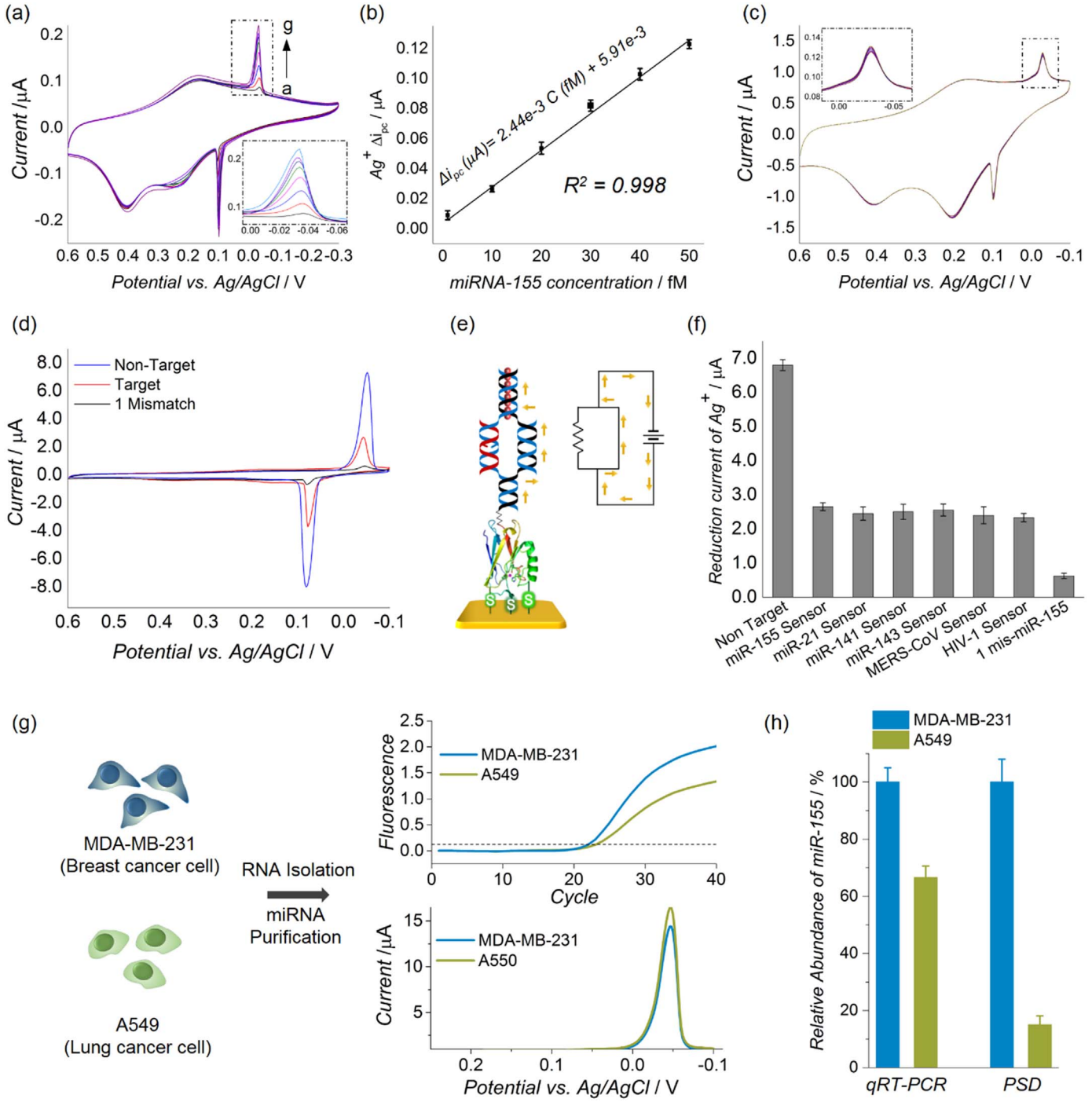

Fig. 4. Sensor performance. (a) CV response of C-8Ag$^+$-C PSD/rAzu for 6 different concentration of miR-155: a) 50fM, (b) 40fM, (c) 30fM, (d) 20fM, (e) 10 fM, (f) 1fM and (g) Probe signal (50fM). (b) The calibration linear curve for the Fig. 4a. (c) Reproducibility test upon 40 cycles of PSD/rAzu at 20 fM of miR-155. Four-cycle increments have been illustrated. (d) CV analysis for non-target miRNA strand, target miR-155 and 1-mismatched base pair miR-155. (e) Schematic illustration of short circuit occurrence in 1-mismatch PSD. (f) Selectivity of the miR-155 sensor for the detection of the non-target strands, miR-155 in the mixture miRNAs and 1-mismatched miR155 and also the capability of the PSD/rAzu structure for the development of different biosensors for the detection of other miRNAs and other viruses; Data was obtained based on three independent experiments. Each strands' concentration was 2 pM, g) The typical qRT-PCR (upper) and PSD biosensor (lower) graphs obtained from MDA-MB-231 and A549 cell lines for the detection of miR-155 expression level; dash line shows the C_t value, (h) The corresponding relative abundance of the miR-155 in the mentioned cell lines by qRT-PCR and PSD biosensor experiments; data was obtained from 3 identical reactions.

silver ions (Ag^+-i_{pc}) in PSD is more than 20% that of the dsDNA. Fig. S7 shows the conductance differences between dsDNA and PSD adsorbed on both an Au electrode and rAzu as a function of DNA concentration. A linear calibration curve is seen for all the two structures of dsDNA/rAzu and PSD/rAzu. By comparing the Ag^+-i_{pc} for PSD (I_2) and dsDNA (I_1) adsorbed on rAzu, the following equation can be extracted:

$$I_2/\mu A = 1.2\, I_1/\mu A + kC,\ \ R^2 = 0.995$$

Where R is the regression coefficient, k equals 0.24 ($\mu A/pM$) and C (pM) is the concentration of DNA immobilized on rAzu. The first term in the equation refers to the classical assumption of 20% current enhancement. The second term may be due to the presence of azurin

protein and the fact that in organic semiconductors there are no conventional valence bands and no delocalized energy states, whereas, they are localized within the whole or part of the organic structure. (Waleed Shinwari et al., 2010) Hence, the spatial arrangement of the molecular orbits would be the key factor for electrons to occupy these states, leading to a nonzero "hopping" probability between energy states. Therefore, PSD might provide new spatial extents of energy states that give rise to the CT efficiency across the molecule.

2.4. Electrical analysis using scanning tunneling microscopy (STM) Break-Junction Technique

To further prove the electrical properties of the individual DNA structures at the nanoscale and more accurate level, STM break-junction technique (Li et al., 2008; Ramnani et al., 2013) was conducted at room temperature. Fig. 3d plots some examples of conductance versus tip separation which indicates the molecular bridge formation of dsDNA and PSD. The conductance of each structure can be measured through the current steps, of which, a notable difference between the conductances of the two structures are evident. Although it is obvious that, for a bare gold there was no current plateau resulting from non-existence of a molecular junction (Fig. S8). The conductance histograms constructed from 500 conductance traces for dsDNA and PSD are also shown in Fig. 3e and f. Considering the conductance formula of $G = I_{plateau} / V_{bias}$ and assuming the $G_0 = 2e^2 / h \approx 77.4\ \mu S$, the average conductance of $1.59 \times 10^{-6}\ G_0$ was calculated for PSD on Au substrate which is about 1.8 times more than that of the dsDNA ($0.87 \times 10^{-6}\ G_0$). The reason for the higher conductance of our studied dsDNA compared with the previous studies (Shapir et al., 2008; Zhang et al., 2014) can be attributed to using a tungsten tip instead of a gold tip. Also, measurement in a non-vacuum state and not using a chemical linker to be attached to the tip may be the cause of high current fluctuations in our data. Even though, the STS data cannot be compared with the electrochemical data, but their result complement each other to prove that PSD is more conductive than dsDNA. Extra analysis are provided in Supplementary information (S. 9) and Fig. S9.

2.5. The principal of electrochemical DNA-based sensor for nucleic acid detection

The proposed PSD structure was developed as a DNA-based electrochemical biosensor for nucleic acid detection. As seen in Fig. 1c, the probe consists of an imperfect PSD adsorbed on rAzu, which lacks a single strand, the target strand (miR-155). The imperfect PSD is not in an upright state due to its higher bending elasticity compared to the perfectly-matched PSD. Therefore, silver ions are closer to the electrode surface, resulting in a higher signal as a consequence of Ag^+ reduction. MiR-155 was added to the probe and incubated for 1 h at RT. Details about optimum assembly time of miRNA on PSD biosensor is provided in Supporting information (S. 10 and Fig. S10). Afterwards, the electrode was directed to the electrochemical cell for CV analysis. In the presence of miR-155, because of the formation of an upright PSD on the rAzu, the detection signal decreased and the correspondent Ag^+-i_{pc} was defined as our detection signal (Fig. 1c). It should be mentioned that, replacement of the T_2 strand with miRNA (R) in PSD resulted in no significant difference in the redox current or behavior of species (Fig. S11). To achieve a higher detection signal and lower limit of detection (LOD), we determined the threshold number of coordinated eight silver ions inside a 22 bp dsDNA of the head part of the PSD (Supplementary information, S. 11 and Fig S. 12).

2.6. Nucleic acid biosensor performance

CV was performed to evaluate the LOD and dynamic range of the electrochemical sensor. As shown in Fig. 4a and b, the electrochemical signal of the reduced Ag^+ increased with increasing miR-155 concentration. The redox signal of rAzu increased with increasing target strand concentration. This indicates greater involvement of copper ions in the electron donation process due to presence of a greater number of electron acceptors (Ag^+ ions). In order to accurately analyze the LOD of the PSD biosensor, 20 µl of the imperfect PSD (sensor probe) at the concentration of 50fM was assembled onto the rAzu modified gold electrode then 20 µl of different miR-155 aliquots at the concentration of 1fM to 50fM were incubated onto the sensor probe for 1 h at RT. After the washing process, electrodes were directed to the electrochemical measurement. As seen in Fig. 4a, the reduction current of silver ion (Ag^+-i_{pc}) increased by reducing the concentration of miRNA from 50fM to 1fM. A corresponding linear graph (Fig. 4.b) was achieved from plotting the Ag^+-i_{pc} difference between the "on" and "off" states (Ag^+-Δi_{pc}) as a function of the miRNA concentration. The Ag^+-Δi_{pc} increased by increasing the target concentration until almost the whole imperfect PSDs were switched and the Ag^+-i_{pc} dropped by ~63% compared to the probe signal. The regression equation was Δi_{pc} (µA) = 2.44e-3C (fM) + 5.91e-3; R^2 = 0.9984, and the LOD was calculated ~0.5 fM (~ 6×10^3 molecules in 20 µl) based on the $3 \times (S/m)$ method, where the S is the standard deviation of the blank signal and m is the slope of the linear fitting curve.

The PSD biosensor results were verified by comparing to the quantitative real-time polymerase chain reaction (qRT-PCR) results (Fig. S13). Primer design and experimental details are provided in supporting information (S. 12). Comparing to the PSD biosensor results, similar performance was observed, however in case of qRT-PCR a C_t value of 39.4 was found for the negative control which may be due to the non-specific bindings between the non-target miRNA and RT primer during cDNA synthesis in reverse transcription process. Also it should be note that, the essential step of reverse transcription along with the primer design complexity undoubtedly cause experimental errors and extra costs to the system.

Repeatability test was performed using 10 probes under identical experimental conditions; the relative standard deviation (RSD) was 3.5%. For reversibility test, 40 cycles of CV measurement were carried out on 20 fM miR-155; a slight decrease in Ag^+-i_{pc} was observed from 492 nA to 471 nA. The RSD was calculated to be 3.2% (Fig. 4c). Alternatively, after storage for 1 week at 4 °C, the sensitivity of the biosensor was unchanged. After 2 weeks, the calculated RSD was 3.1%. These results show that our PSD biosensor displayed an acceptable Stability.

The specificity of the proposed electrochemical sensor was verified by introducing single-base-pair mismatched and non-complementary RNA and DNA targets. Interestingly, addition of a target RNA strand with a single mismatched base pair resulted in a significant drop of ~ 88% in the probe signal (Fig. 4d). This can be described as the short-circuit law in classical physics which affirms that, in a parallel electrical circuit having two paths of current flow, current travels along the path with no electrical impedance. Therefore, the single mismatched duplex can be thought of as a path with higher impedance than the other parallel duplex (Fig. 4e). As a result, in the presence of a single mismatched base target, current would flow through the other parallel strand, yielding a lower Ag^+-i_{pc}. Indeed, the parallel part of the PSD/PSD disrupts the base pairs' π-stacks, which are the CT bridge in dsDNA (Kelley and Barton, 1999), however as mentioned above, intercalation of two small strands (T_1 and T_2/R) into the structure might provide a new spatial state of energy that can compensate for the π-π orbital loss in dsDNA and support higher mobility and charge delocalization. Therefore, the presence of single mismatch at one side of PSD prohibits the CT across the damaged helix, which might distract electron coupling of the two parallel helices and lead to a lower conductance. As seen in Fig. 4f, non-complementary RNA and DNA strands were also introduced to our sensor, which resulted in a higher signal than that of miR-155 due to the higher bending flexibility of the imperfect PSD. Furthermore, versatility test was carried out upon

different DNA and RNA targets. As seen in Fig. 4f, five different sensors were developed (see table S3 for the primer design) and employed to detect their specified targets of miR-21, miR-141, miR-143, MERS-CoV and HIV-1. The results showed a proper response of our sensing strategy for the general detection of different types of target nucleic acids. The small deviation in signals can be interpreted as the different numbers of G/C contents in different target strands.

In order to further investigate the credibility of our PSD biosensor for the detection of microRNA in clinical samples, the expression level of miR-155 in two different cancer cell lines of MDA-MB-231 (breast cancer cell) and A549 (lung cancer cell) was monitored and the result was compared with qRT-PCR and previous reports (Lee et al., 2014). In this regard, the total microRNAs of ~90 ng was isolated and purified from both above-mentioned cell lines (details in supporting information, S. 13). Same amount of the total miRNAs were used for both PSD biosensor and qRT-PCR and the results for three independent samples were recorded. As seen in Fig. 4g, similar results were obtained from both techniques. The level of miR-155 from MDA-MB-231 and A549 was measured on the basis of the standard curves obtained from qRT-PCR and PSD biosensor using serial dilution of the synthetic miR-155 (Fig. S13b and d). The results showed a higher expression level of miR-155 in MDA-MB-231 cell line compared to the A549, which is in a good agreement with the previous studies (Lee et al., 2014). By normalizing the miR-155 expression level, the abundance of this oncogene was plotted in Fig. 4. h. Notably, in the case of PSD biosensor, the difference between the levels of miR-155 is a bit higher and more distinguishable than that of the qRT-PCR results. This may be ascribed to the RNA extraction variation or non-specific binding of stem-loop RT primer which results in non-target reverse transcription following the amplification errors. As a result, our data proved that the PSD biosensor is quite capable of miRNA profiling in real samples.

3. Conclusion

The PSD/rAzu hybrid was developed and applied for a label-free, ultrasensitive and facile electrochemical-based nucleic acid biosensor with fast response and high fidelity to discriminate single-mismatched and non-complementary targets. Assuming as a classical parallel electrical circuit, the PSD undertook a higher conductivity than dsDNA. The electrical conductance of PSD and DNA structures were investigated by STS and CV techniques based on the alteration of silver ions reduction which was intercalated between C-C mismatches. Having higher conductivity of PSD compared with dsDNA gave rise to the sensitivity of our biosensor. Furthermore, rAzu functioned as a selective molecule to accurately control the number of DNAs together with their vertical arrangement as well as providing enough spacing for reliable and fast structure transformation resulting from target detection. Likewise, the PSD/rAzu structure was investigated theoretically to further understand the charge transfer mechanism across the biomolecules. The proposed DNA/RNA/protein hybrid structure promises various potential applications such as nanoscale biomedical device and bioelectronics devices as the electrical element to regulate the signal at single molecular level.

Acknowledgement

This research was supported by Leading Foreign Research Institute Recruitment Program through the National Research Foundation of Korea (NRF) funded by the Ministry of Science, ICT & Future Planning (MSIP) (2013K1A4A3055268) and by the National Research Foundation of Korea (NRF) grant funded by the Korea government (MSIP) (No. 2014R1A2A1A10051725) and by Basic Science Research Program through the National Research Foundation of Korea(NRF) funded by the Ministry of Education (2016R1A6A1A03012845).

Appendix A. Supporting information

Supplementary data associated with this article can be found in the online version at doi:10.1016/j.bios.2017.07.005.

References

Baker, M., 2006. Nat. Biotech. 24 (8), 931–938.
Bard, A.J., Faulkner, L.R., 2000. Electrochemical Methods: Fundamentals and Applications Second ed.. John Wiley & Sons, New York.
Calin, G.A., Croce, C.M., 2006. Nat. Rev. Cancer 6 (11), 857–866.
Campuzano, S., Torrente-Rodríguez, R.M., López-Hernández, E., Conzuelo, F., Granados, R., Sánchez-Puelles, J.M., Pingarrón, J.M., 2014. Angew. Chem. Int. Ed. 53 (24), 6168–6171.
Catuogno, S., Esposito, C.L., Quintavalle, C., Cerchia, L., Condorelli, G., De Franciscis, V., 2011. Cancers 3 (2), 1877–1898.
Chen, G., Shen, Y., Xu, T., Ban, F., Yin, L., Xiao, J., Shu, Y., 2016. Biosens. Bioelectron. 77, 1020–1025.
Cheng, Y., Zhang, X., Li, Z., Jiao, X., Wang, Y., Zhang, Y., 2009. Angew. Chem. Int. Ed. 48 (18), 3268–3272.
Choi, J.-H., Lee, J., Shin, W., Choi, J.-W., Kim, H.J., 2016. Nano Converg. 3 (1), 24.
Choi, J.-W., Oh, B.-K., Kim, Y.J., Min, J., 2007. Appl. Phys. Lett. 91 (26), 263902.
Chung, Y.-H., Lee, T., Yoo, S.-Y., Min, J., Choi, J.-W., 2015. Sci. Rep. 5, 14501.
Corgier, B.P., Laurent, A., Perriat, P., Blum, L.J., Marquette, C.A., 2007. Angew. Chem. Int. Ed. 46 (22), 4108–4110.
Drummond, T.G., Hill, M.G., Barton, J.K., 2003. Nat. Biotech. 21 (10), 1192–1199.
Dupont-Filliard, A., Roget, A., Livache, T., Billon, M., 2001. Anal. Chim. Acta 449 (1–2), 45–50.
Feng, X., Gan, N., Zhang, H., Li, T., Cao, Y., Hu, F., Jiang, Q., 2016. Biosens. Bioelectron. 75, 308–314.
Ge, Z., Lin, M., Wang, P., Pei, H., Yan, J., Shi, J., Huang, Q., He, D., Fan, C., Zuo, X., 2014. Anal. Chem. 86 (4), 2124–2130.
He, L., Thomson, J.M., Hemann, M.T., Hernando-Monge, E., Mu, D., Goodson, S., Powers, S., Cordon-Cardo, C., Lowe, S.W., Hannon, G.J., Hammond, S.M., 2005. Nature 435 (7043), 828–833.
Hong, B.J., Oh, S.J., Youn, T.O., Kwon, S.H., Park, J.W., 2005. Langmuir 21 (10), 4257–4261.
Inouye, M., Ikeda, R., Takase, M., Tsuri, T., Chiba, J., 2005. Proc. Natl. Acad. Sci. USA 102 (33), 11606–11610.
Jiang, J., Lee, E.J., Gusev, Y., Schmittgen, T.D., 2005. Nucleic Acids Res. 33 (17), 5394–5403.
Jiang, Z., Wang, H., Zhang, X., Liu, C., Li, Z., 2014. Anal. Methods 6 (23), 9477–9482.
Kafi, M.A., Cho, H.-Y., Choi, J.-W., 2016. Nano Converg. 3 (1), 17.
Kelley, S.O., Barton, J.K., 1999. Science 283 (5400), 375–381.
Labib, M., Khan, N., Berezovski, M.V., 2015. Anal. Chem. 87 (2), 1395–1403.
Labib, M., Sargent, E.H., Kelley, S.O., 2016. Chem. Rev. 116 (16), 9001–9090.
Labib, M., Khan, N., Ghobadloo, S.M., Cheng, J., Pezacki, J.P., Berezovski, M.V., 2013. J. Am. Chem. Soc. 135 (8), 3027–3038.
Lee, H., Park, J.-E., Nam, J.-M., 2014. Nat. Commun. 5, 3367.
Lee, T., Kim, S.-U., Min, J., Choi, J.-W., 2010. Adv. Mater. 22 (4), 510–514.
Lee, T., Min, J., Kim, S.-U., Choi, J.-W., 2011. Biomaterials 32 (15), 3815–3821.
Li, C., Li, Z., Jia, H., Yan, J., 2011. Chem. Commun. 47 (9), 2595–2597.
Li, D., Jiang, C., Jiang, J., Ren, X., 2008. Mater. Chem. Phys. 111 (1), 168–171.
Lin, M., Song, P., Zhou, G., Zuo, X., Aldalbahi, A., Lou, X., Shi, J., Fan, C., 2016. Nat. Protoc. 11 (7), 1244–1263.
Ma, Z., Ma, Y., Xia, Q., Li, Y., Li, R., Chang, W., Chen, J., Leng, Z., Tao, K., 2016. J. Cancer Res. Clin. Oncol., 1–12.
Millikan, R.A., Bishop, E.S., 1917. Elements of Electricity. American Technical Society, Chicago.
Nolan, T., Hands, R.E., Bustin, S.A., 2006. Nat. Protoc. 1 (3), 1559–1582.
O'Connell, R.M., Rao, D.S., Chaudhuri, A.A., Boldin, M.P., Taganov, K.D., Nicoll, J., Paquette, R.L., Baltimore, D., 2008. J. Exp. Med. 205 (3), 585–594.
Ono, A., Cao, S., Togashi, H., Tashiro, M., Fujimoto, T., Machinami, T., Oda, S., Miyake, Y., Okamoto, I., Tanaka, Y., 2008. Chem. Commun. (39), 4825–4827.
Ramnani, P., Gao, Y., Ozsoz, M., Mulchandani, A., 2013. Anal. Chem. 85 (17), 8061–8064.
Roa, W., Brunet, B., Guo, L., Amanie, J., Fairchild, A., Gabos, Z., Nijjar, T., Scrimger, R., Yee, D., Xing, J., 2010. Clin. Invest. Med. 33 (2), E124–E132.
Shapir, E., Cohen, H., Calzolari, A., Cavazzoni, C., Ryndyk, D.A., Cuniberti, G., Kotlyar, A., Di Felice, R., Porath, D., 2008. Nat. Mater. 7 (1), 68–74.
Shi, L., Chu, Z., Liu, Y., Jin, W., Chen, X., 2013. Biosens. Bioelectron. 49, 184–191.
Slinker, J.D., Muren, N.B., Gorodetsky, A.A., Barton, J.K., 2010. J. Am. Chem. Soc. 132 (8), 2769–2774.
Song, K.-S., Balasaheb Nimse, S., Kim, J., Kim, J., Nguyen, V.-T., Ta, V.-T., Kim, T., 2011. Chem. Commun. 47 (25), 7101–7103.
Válóczi, A., Hornyik, C., Varga, N., Burgyán, J., Kauppinen, S., Havelda, Z., 2004. Nucleic Acids Res. 32 (22), (e175-e175).
Waleed Shinwari, M., Jamal Deen, M., Starikov, E.B., Cuniberti, G., 2010. Adv. Funct. Mater. 20 (12), 1865–1883.
Walker, G.T., Fraiser, M.S., Schram, J.L., Little, M.C., Nadeau, J.G., Malinowski, D.P., 1992. Nucleic Acids Res. 20 (7), 1691–1696.
Wang, H.-N., Crawford, B.M., Fales, A.M., Bowie, M.L., Seewaldt, V.L., Vo-Dinh, T., 2016a. J. Phys. Chem. C 120 (37), 21047–21055.
Wang, Q., Liu, R., Yang, X., Wang, K., Zhu, J., He, L., Li, Q., 2016b. Sens. Actuators B: Chem. 223, 613–620.
Wohlgamuth, C.H., McWilliams, M.A., Slinker, J.D., 2013. Anal. Chem. 85 (18), 8634–8640.
Wu, L., Qu, X., 2015. Chem. Soc. Rev. 44 (10), 2963–2997.
Wu, X., Chai, Y., Zhang, P., Yuan, R., 2015. ACS Appl. Mater. Interfaces 7 (1), 713–720.
Yagati, A.K., Lee, T., Min, J., Choi, J.-W., 2013. Biosens. Bioelectron. 47, 385–390.
Yin, B.-C., Liu, Y.-Q., Ye, B.-C., 2012. J. Am. Chem. Soc. 134 (11), 5064–5067.
Zhang, X., Wang, Y., Fricke, B.L., Gu, L.-Q., 2014. ACS Nano 8 (4), 3444–3450.